Progress In Electromagnetics Research B, Vol. 102, 131–149, 2023

The Effect of Magnet Pole Unequal Thickness on Axial Flux Motor Tooth Groove Torque

Jianwei Liang[1], Xinhua Wang[1, *], Peiyao Guo[1], Huan Liu[1], Xuchang Yuan[1], and Dong Chen[2]

Abstract—To address the problems of torque ripple, vibration, and noise generated by cogging torque in a dual-stator single-rotor axial magnetic field permanent magnet motor, this article adopts an unequal thickness pole structure to reduce cogging torque. At first, the process of cogging torque generation is analyzed, followed by an examination of the mathematical formulation of cogging torque using the energy technique and Fourier decomposition method. Then, the impacts of several pole optimization approaches on cogging torque reduction are then compared, and the findings are investigated using the finite element method to demonstrate the efficiency of the optimization method. The results show that the optimization effect of unequal thickness pole structure is the best. Lastly, the optimized motor's air-gap flux density, counter-electromotive force, harmonic content, and rotor mechanical strength were compared and studied to demonstrate that the unequal-thickness structure used in this research can increase motor performance. Finally, based on the determined motor parameters, experimental study of the prototype was carried out to verify the correctness of the motor structure and analysis.

1. INTRODUCTION

Axial field permanent magnet (AFPM) motors are also called disk permanent magnet motors. Different from traditional radial motors, AFPM motors have a radial plane air gap structure with an axial air gap flux direction. Compared to radial flux motors [1, 2], axial motors have no losses in the excitation system [3], and the motor works more efficiently [4]. The symmetrical arrangement of the stator and rotor facilitates the heat dissipation of stator windings [5]. It also has the advantages of low vibration noise [6], simple assembly, and high efficiency [7]. Such motors have broad application prospects in automotive drives, flywheel energy storage systems, aerospace, industrial equipment needs, and wind power generation [8–10].

The disc permanent magnet motor has a variety of structural forms. According to the number of stators and rotors as well as their relative positions, they can be roughly divided into four types: single stator and single rotor structure, double rotor intermediate stator structure, double stator intermediate rotor structure, and multi-disc structure [11, 12]. Depending on the mounting position of the permanent magnet, it can be divided into two types: stator permanent magnet type and rotor permanent magnet type. The stator AFPM motor is a salient pole rotor structure. The permanent magnet of the motor is located in the stator yoke or stator teeth, which is suitable for high-speed operation. It has the features of compact structure, reliable operation, wide speed range, and easy cooling [13]. However, this structure of the motor also has some problems, such as low utilization of permanent magnets, serious magnetic leakage, and large torque fluctuations. Compared with the stator PM structure, the rotor AFPM motor has a wider range of applications and has been studied for a longer period of time.

Received 23 April 2023, Accepted 4 August 2023, Scheduled 18 August 2023

* Corresponding author: Xinhua Wang (1066549216@qq.com).

[1] School of Electrical Engineering and Automation, Jiangxi University of Science and Technology, Ganzhou 341000, China.

[2] Hangzhou Zhonghao Electric Technology Cd Ltd, Hangzhou 310000, China.

The permanent magnets of rotor AFPM motors are usually of surface mounted construction, with the permanent magnets attached to the surface of the rotor core. In this motor structure, the motor rotor has problems such as unbalanced axial suction and large flux leakage at the rotor end [14, 15], which in turn causes problems such as high cogging torque [16] and severe reduction in power density [17, 18]. Because of the wide application of this kind of motor, many experts and scholars have done a lot of research on the rotor permanent magnet motor and proposed many solutions to its problems [19, 20].

Reference [21] designed a structure and magnetic circuit of an axial-flow permanent magnet brushless DC motor with unequal-thickness curved permanent magnets, and a three-dimensional analytical model was built using Maxwell 3D. The air gap flux density, reverse electromotive force and torque of the motor are analyzed to verify the correctness of the model and design. Ni et al. of Hefei University of Technology used an analytical method to analyze unequal thick magnetic poles and proved the feasibility of the method [22, 23]. Li et al. of Qingdao University performed analytical calculations on the magnetic pole fractionation and pole unequal thickness structure [24]. These references verify that the pole unequal thickness structure is effective in weakening the motor cogging torque.

The research object of this paper is a double-stator single-rotor axial flux permanent magnet (AFIR) motor. The double stator structure can be better designed for cooling on the stator end caps, which facilitates the heat dissipation of the motor [25]. As with conventional radial motors, these motors suffer from significant torque fluctuations and large cogging torque problems during operation. In this paper, a 10-pole 45-slot AFIR motor with a power of 45 kW is used as a prototype model. Fig. 1 shows the 1/5 simulation model of the motor. According to the unit motor theory, a 10-pole, 45-slot AFIR motor can be considered as consisting of five 2-pole, 9-slot unit motors. Therefore, to save time in motor simulation, only 1/5 model of AFIR motor needs to be analyzed.

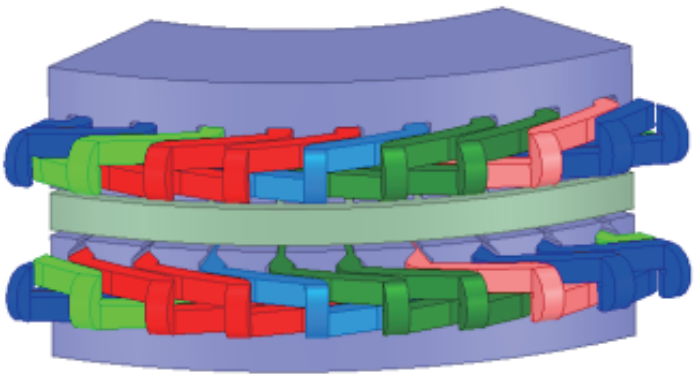

Figure 1. Simulation model diagram.

This paper analyzes the causes of cogging torque generated by AFIR motors. In order to solve the problem of large cogging torque, an analysis of cogging torque is carried out. According to the mathematical formula obtained by analysis, the optimization is carried out from one of the amplitudes B_{rn} (the Fourier decomposition coefficient of the square of the air gap magnetic density generated by the permanent magnet) that affects the cogging torque, and the optimization of the magnetic pole parameters is the main factor affecting B_{rn}. In this paper, various optimization methods are carried out for rotor permanent magnet poles, including axial splitting of permanent magnets, radial splitting of permanent magnets, and unequal thickness structure of permanent magnets, and the optimization effects of various optimization methods are compared. The two methods, axial segmentation and radial segmentation, are not as effective in weakening the cogging torque of the motor, and the cogging torque decreases less. The rotor permanent magnets are of unequal thickness, and the output torque of the motor is not reduced but slightly increased. Also, the torque fluctuation and cogging torque are better optimized. Finally, an unequal-thickness pole structure was selected to optimize the motor, and the air-gap flux density distribution, counter-electromotive force waveform and its harmonic analysis, and rotor mechanical strength of the motor before and after optimization were compared and analyzed.

Aiming at minimum cogging torque, the optimal combination of thicknesses of unequal-thickness pole structures is determined with a certain accuracy (0.01 mm) to ensure the performance of AFIR motors.

2. ANALYSIS OF MOTOR TOPOLOGY AND OPTIMIZATION METHODS

2.1. AFIR Motor Topology

Conventional surface mount AFIR motors usually have a parallel stator slot structure for the stator and rotor, and a trapezoidal structure for the permanent magnets. Fig. 2 shows the topology of AFIR motor, which consists of two identical rotors and an intermediate stator. Table 1 is the initial design parameters of the motor.

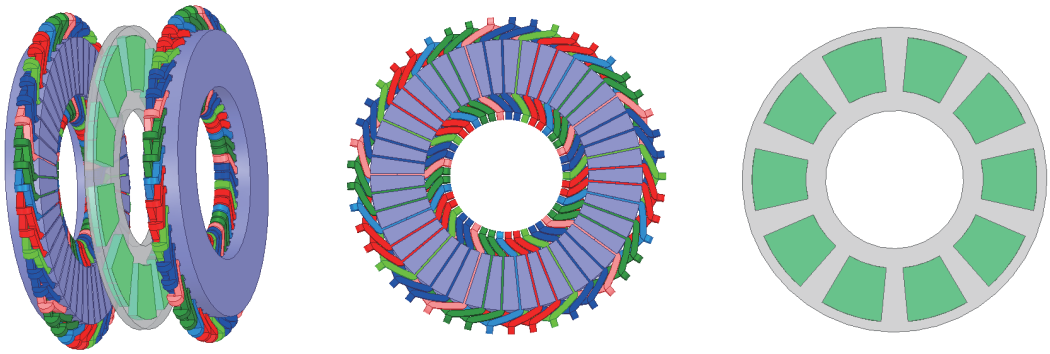

Figure 2. Motor topology.

Table 1. Initial design parameters.

Motor parameters	Numeric value
Stator outer diameter/mm	240
Stator inner diameter/mm	145
Rotor outer diameter/mm	270
Rotor inner diameter/mm	115
Air gap/mm	2
Number of stator slots	45
Number of pole pairs P	5
Permanent magnet type	Ndfe35
Permanent magnet length/mm	45
Permanent magnet thickness/mm	8

2.2. Comparison of Different Optimization Methods

Unlike ordinary AFPM motors where the permanent magnets are surface mounted, the permanent magnets of AFIR motors are embedded in the rotor disk, which effectively reduces the axial length of the motor. The rotor disk is composed of a permanent magnet and a rotor core. The thickness of the permanent magnets in the initial structure of the rotor is uniform, and the thickness of the permanent magnets in the middle of the unequal-thickness pole structure is greater than that of the sides. As shown in Fig. 3, Fig. 3(a) is the initial structure, and Fig. 3(b) is an unequal thickness magnetic pole structure. Fig. 4 shows the flowchart for the specific design and optimization of the AFIR motor.

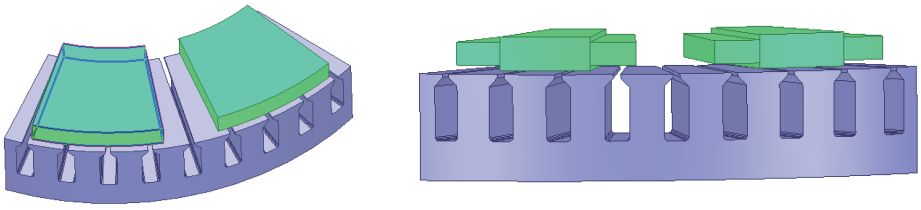

Figure 3. Different rotor structures.

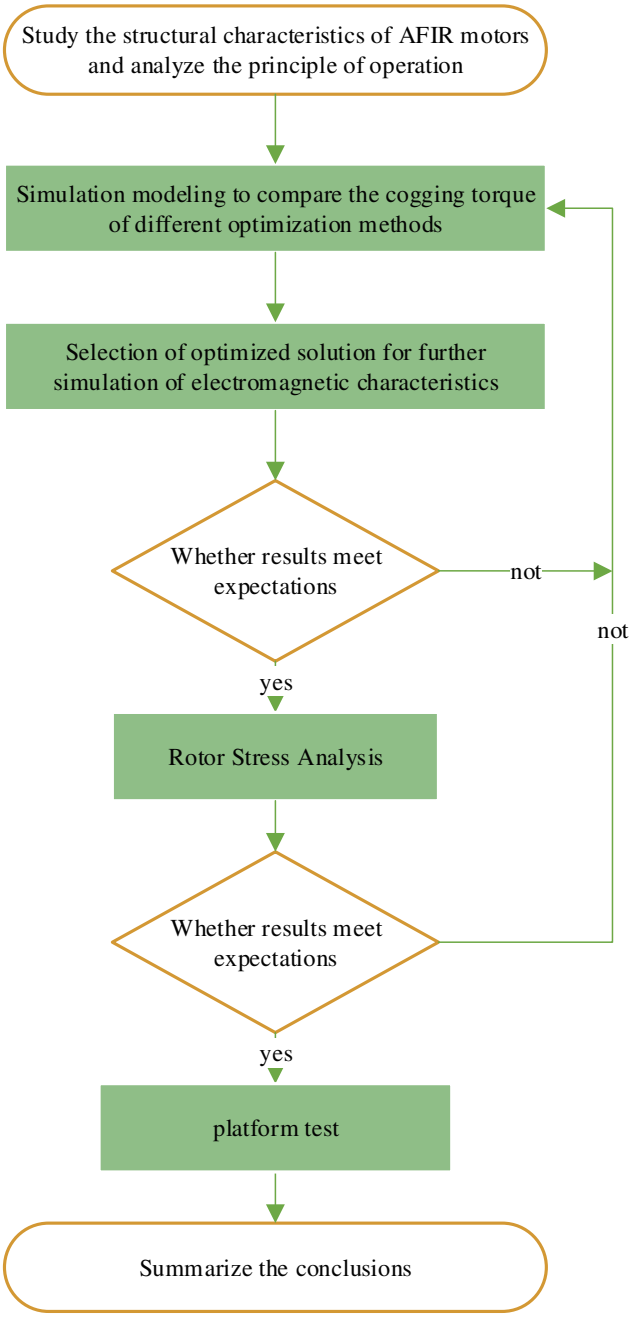

Figure 4. Flowchart.

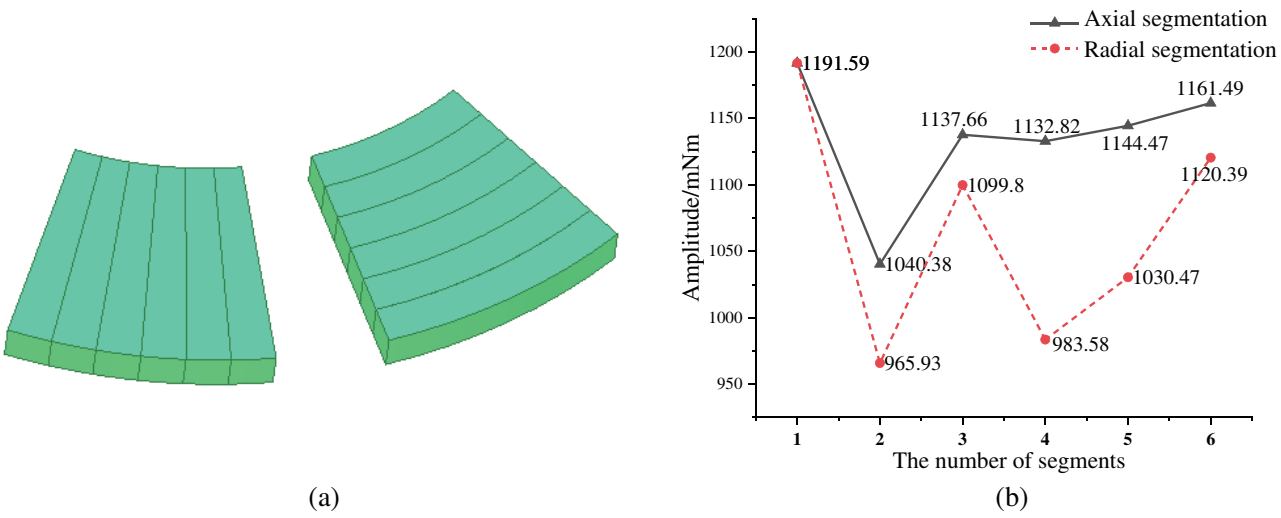

Figure 5. Axial versus radial segmentation. (a) Segmentation example. (b) Torque amplitude of cogging.

The effect of axial and radial segmentation of the magnetic pole on the torque amplitude of the tooth slot is shown in Fig. 5. Fig. 5(a) shows the effect of axial and radial segmentation, and only the example diagram divided into six segments is shown in the figure. Fig. 5(b) is the influence of the number of magnetic pole segments on the amplitude of the cogging torque. It can be seen from the figure that the pole segmentation has an effect on the weakening of the cogging torque. As the number of pole segments increases, the variation of cogging torque first decreases and then increases. According to the graph, the axially segmented cogging torque can be reduced by up to 12.6% and by as little as 2.5%. Radial segmentation can be weakened by 19.1%, with a minimum of 6%. It can be seen that for the same number of segments, the radial segments weaken the tooth groove torque more than the axial segments.

Figure 6 shows a comparison of the cogging torque curves and torque pulsation curves for different rotor configurations. From the figure, it can be seen that the axial and radial segmentation of the pole can serve to attenuate the cogging torque and reduce the torque fluctuation, but the optimization effect is limited, and the unequal-thickness pole has the best effect.

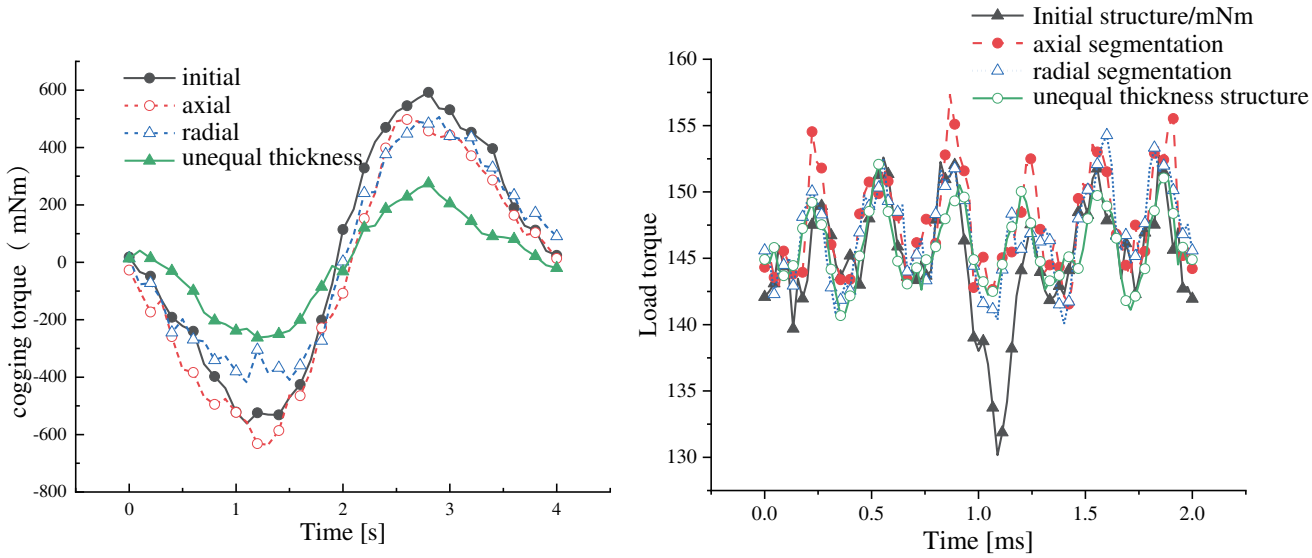

Figure 6. Cogging torque and load torque.

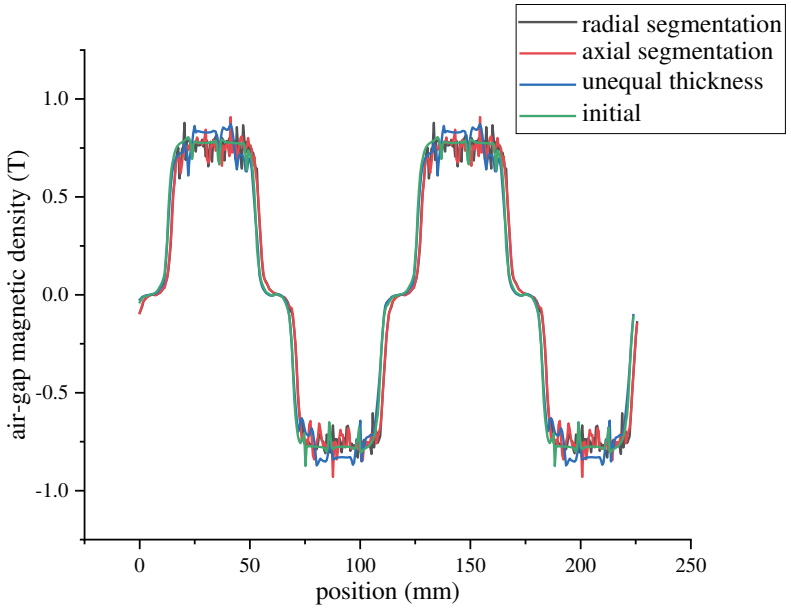

Figure 7. Air-gap magnetic density for different topologies.

The simulation curves of air gap magnetization for different topologies are shown in Fig. 7. By the comparison in Fig. 7, it is found that the air gap magnetic density of unequal thickness structures is sinusoidal.

From the previous analysis, it is clear that radial segmentation is superior to axial segmentation under the same conditions. Therefore, in this paper, based on the radial segmentation of the magnetic poles, the poles are changed to unequal thickness structure to study its weakening effect on the cogging torque of the AFIR motor and its effect on other electromagnetic characteristics.

3. GEAR TORQUE OF THE MOTOR

3.1. Mechanism of Cogging Torque

The cogging torque can be known from its name, which is related to the stator slotting, and it exists only in permanent magnet motors. Cogging torque is a unique property of permanent magnet motors and refers to the reluctance torque generated by the interaction between the stator cogs and rotor magnets when the motor windings are not energized. The cogging torque is also known as the positioning torque because it tries to hold the rotor magnet in a certain position, which will greatly affect the control accuracy of the motor. The cogging torque is defined as the negative derivative of the magnetic field energy W with the relative position angles α of the stator and rotor when the motor is not turned on.

$$T_{\text{cog}} = -\frac{\partial W}{\partial \alpha} \tag{1}$$

3.2. Analytical Analysis of Cogging Torque

For the purpose of analysis, the following assumptions were made about the structure and relevant parameters of the AFIR motor [26].

1. The permeability of the armature tends to infinity.
2. With the exception of pole optimization, permanent magnets are identical in shape and size and evenly distributed.
3. The core-stacking coefficient is approximately 1.
4. The rotor teeth and stator groove widths are the same at each radius.

As shown in Fig. 8(a), the position of $\theta = 0$ is set on the pole centroid line. α is called the relative position angle of the stator and rotor and refers to the angle between the centerline of a particular tooth and the centerline of a particular permanent magnet pole.

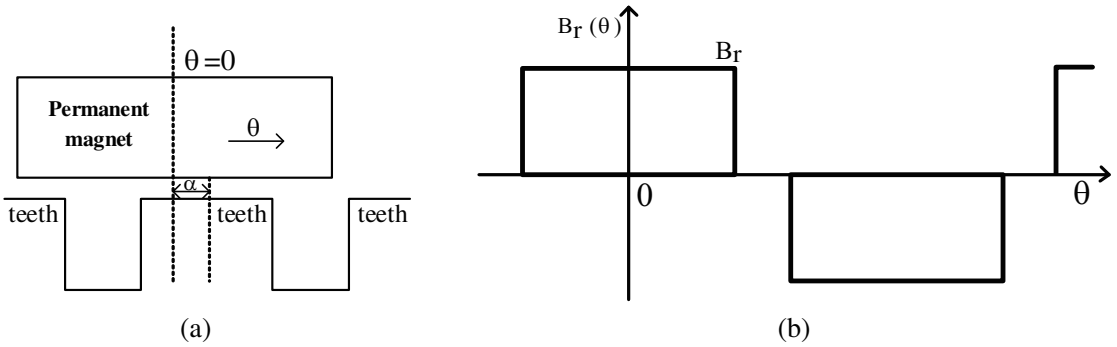

Figure 8. Groove torque generation mechanism.

According to hypothesis 1, the magnetic field energy stored in the AFIR motor is approximately equal to the sum of the magnetic field energy stored in the permanent magnet and the air gap of the motor:

$$W \approx W_{airgap+PM} = \frac{1}{2\mu_0}\int_V B^2 dV \tag{2}$$

where $W_{airgap+PM}$ denotes the sum of the energy stored in the air gap and the permanent magnet, μ_0 the vacuum permeability $\mu_0 = 4\pi \times 10^{-7}$ H/m, and B the magnetic induction.

The distribution of air gap magnetic density along the armature surface of an AFIR motor can be expressed as

$$B(\theta, \alpha) = B_r(\theta)\frac{h_m(\theta)}{h_m(\theta) + \delta(\theta, \alpha)} \tag{3}$$

In the above formula, $B_r(\theta)$ is the residual magnetic density of the permanent magnet, $h_m(\theta)$ the distribution along the circumference of the permanent magnet magnetization direction length, and $\delta(\theta, \alpha)$ the effective length of the air gap. Formula (3) is substituted into formula (2) to obtain the following equation:

$$W\frac{1}{2\mu_0}\int_V B_r^2(\theta)\left[\frac{h_m(\theta)}{h_m(\theta) + \delta(\theta, \alpha)}\right]^2 dV \tag{4}$$

According to hypothesis 2, the permanent magnets in the AFIR motor are considered uniformly distributed, and Fig. 8(b) shows the distribution of the residual magnetic density of the permanent magnets along the circumference. $B_r^2(\theta)$ is expanded by Fourier on the interval $[-\pi/2p, \pi/2p]$.

$$B_r^2(\theta) = B_{r0} + \sum_{n=1}^{\infty} B_{rn}\cos 2np\theta \tag{5}$$

$B_{r0} = \alpha_p B_r^2$; $B_{rn} = \frac{2}{n\pi}B_r^2 \sin n\alpha_p\pi$; p is the number of pole logarithms; B_r is the permanent magnet remanence; α_p is the polar arc coefficient of the permanent magnet pole.

$$\left[\frac{h_m(\theta)}{h_m(\theta) + \delta(\theta, \alpha)}\right]^2 = G_0 + \sum_{n=1}^{\infty} G_n \cos nz(\theta + \alpha) \tag{6}$$

Substituting formula (4), (5), and (6) into formula (1) can be used to obtain the expression of AFIR motor cogging torque:

$$T_{cog} = \frac{\pi z L_a}{4\mu_0}(R_2^2 - R_1^2)\sum_{n=1}^{\infty} nG_n B_{r\frac{nz}{2p}} \sin nz\alpha \tag{7}$$

where z represents the number of motor slots; L_a is the axial length of the core; R_1 is the outer radius of the armature; R_2 is the radius inside the stator yoke; n is to make $nz/2p$ integer to integer; $\frac{\pi z L_a}{4\mu_0}(R_2^2 - R_1^2)$ is the motor structure parameter [27]. Changing the structural parameters of the motor will lead to a large change in the shape and size of the motor, affecting the overall performance of the motor and increasing the production cost. When the motor is optimized, the structural parameters of the motor are usually not changed. B_{rn} is the Fourier decomposition coefficient of the square of the air gap magnetic density generated by the permanent magnet; G_n is the Fourier decomposition coefficient of the square of the relative air gap magnetic conductivity. It can be seen from formula (7) that the magnitude of the cogging torque is related to the amplitude of G_n and B_{rn}. Changing the pole parameter can change the amplitude of B_{rn}, and changing the armature parameter can change the amplitude of G_n.

In this paper, by reducing the amplitude of B_{rn}, the cogging torque of AFIR motor is weakened, and the axial segmentation of magnetic poles, radial segmentation of magnetic poles, and unequal thickness of magnetic poles are mainly adopted, and the effects of these methods are compared.

4. WEAKENING OF COGGING TORQUE BY UNEQUAL THICKNESS POLES

4.1. Unequal Thickness Pole Structure

By changing the shape of the permanent magnet, the permanent magnet pole is designed into an unequal thickness structure, and B_{rn} can reduce the cogging torque.

With poles of unequal thickness, the permanent magnet is eccentric, as shown in Fig. 9. Using unequal thickness structure, the inner and outer surface centers of permanent magnets are different. The outer diameter corresponds to the center of the circle O', and the radius is R_0. The inner diameter corresponds to the center of the circle with O and the radius R_1. $h'_m(\theta)$ changes with the position angle θ. The eccentricity h is the distance between O and O', and the distribution of the radial component of the air gap magnetic density changes with the change of h.

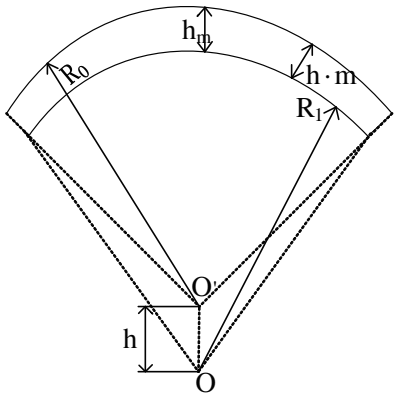

Figure 9. Unequal thickness structures.

It can be seen from the figure that $h = R_1 + h_m - R_0$, h is the difference between the inner and outer radii of the magnetic pole, also known as the magnetic pole eccentricity, and h, $h'_m(\theta)$, and $\delta'(\theta)$ will also change. h_c is the uneven coefficient of the magnetic pole surface, and the expression is as follows [28]:

$$h_c = \frac{R_1 + h_m}{R_0} + \frac{R_1 + h_m}{R_1 + h_m - h} \tag{8}$$

According to the above equation, h_c increases with the increase of h; therefore, the use of unequal thickness poles will affect the magnetization thickness of the permanent magnet, which in turn affects the cogging torque. With a reasonable design of the thickness of the permanent magnet, the cogging torque can be weakened.

When the thicknesses of permanent magnet are the same, the radial distribution of air gap flux density of AFIR motor is the same as that of formula (3). When the thicknesses of the magnetic poles are not equal, the radial component of the air gap magnetic density can be expressed as:

$$B'(\theta) = B_r(\theta)\frac{h'_m(\theta)}{h'_m(\theta)+\delta'(\theta)} = \frac{h'_m(\theta)}{h_m}B_r(\theta)\frac{h_m}{h_m+\delta(\theta)}\,B'_{\mathrm{r}}(\theta)\frac{h_m}{h_m+\delta(\theta)} \tag{9}$$

where $B'_r(\theta) = \frac{h'_m(\theta)}{h_m}B_r(\theta)$, and $B_r(\theta)$ is the residual density of the permanent magnet.

Substituting formulas (9), (4), and (5) into formula (1), we can obtain the expression for the tooth slot torque under unequal thickness poles:

$$T_{cog} = \frac{\pi z L_a}{4\mu_0}(R_2^2 - R_1^2)\sum_{n=1}^{\infty} nG'_n B'_{rn}\sin nz\alpha \tag{10}$$

Comparison of formula (10) with formula (7) shows that the expression for the cogging torque of unequally thick poles is similar to the initial structure, but with different coefficients. Fig. 10 shows the traditional structure and unequal thickness pole structure of the rotor permanent magnet of AFIR motor. On the basis of radial segmentation of permanent magnets, the thickness of magnetic poles adopts a structure with high center and low sides. The initial magnetic pole is uniformly divided into four parts along the radial direction. The unequal thickness structure occupies the middle two parts, and the thickness of the middle is higher than the sides. In order to minimize the effect on the output torque of the motor, this paper chooses an unequal thickness pole structure while keeping the total number of permanent magnets constant.

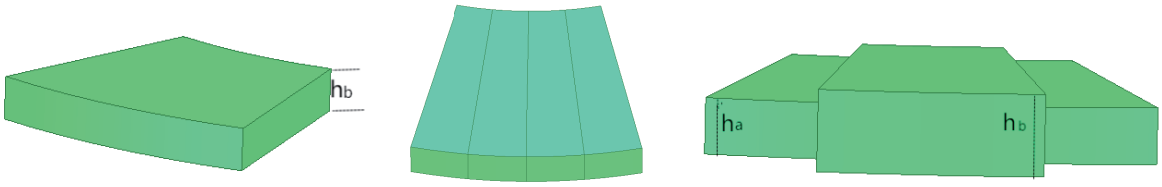

Figure 10. Permanent magnet structure.

It is assumed that the thickness of the initial permanent magnet and the middle part of the improved unequal thickness pole structure are represented by h_b, and the thickness of the permanent magnets on both sides of the unequal thickness poles is represented by h_a.

The initial permanent magnet thickness is 8 mm, in order to ensure that the output torque is not affected by the amount of permanent magnet, letting $h_a + h_b = 16$ mm. The air gap length between the original stator and rotor of the motor is 2 mm. If the thickness of the permanent magnet is too large, the air gap length will be greatly reduced, and the performance of the motor will be greatly changed. So the maximum thickness of h_b should not exceed 9.5 mm, that is, the length of the air gap should be ensured as not less than 5/8 of the original.

Similar to a power source, a permanent magnet can be considered as a magnetic source that continuously provides magnetic power to the outside world. The permanent magnet connects the magnetic material (silicon steel sheet) to form a circuit that creates a magnetic flux, and the magnitude of the flux is related to the magnetic momentum force. The amount of magnetomotive force that a permanent magnet can provide depends on the thickness in the direction of excitation. The thicker the permanent magnet is, the greater the magnetomotive force it can provide, and the greater the magnetic flux is generated.

The equivalent diagram of the magnetomotive force of the two different structures is shown in Fig. 11. The entire permanent magnet is discrete into one parallel permanent magnet. Each permanent magnet faces one part of the air gap. Ignoring the stator slot, the magnetic density of the air gap area is proportional to the thickness of the corresponding permanent magnet. If the thickness of the permanent magnet is equal everywhere, then it produces an air gap magnetization waveform that is

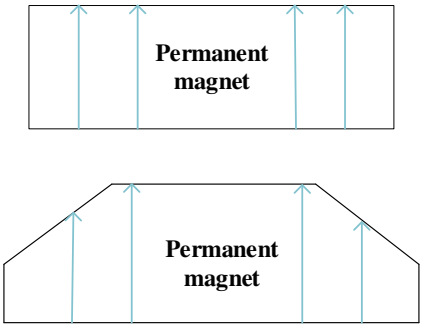

Figure 11. Magnetomotive force equivalence diagram.

uniformly distributed along the surface of the permanent magnet, and if the thickness changes, the air gap magnetization will also change.

4.2. Equivalent Magnetic Network

To better understand the role of each part of the AFIR motor with unequal thickness structure in the magnetic circuit, the equivalent magnetic network diagram of the motor magnetic circuit is analyzed [29, 30]. Fig. 12 shows the equivalent magnetic circuit structure diagram of AFIR motor, where R_{ry} is rotor yoke reluctance; $Rm1$ and $Rm2$ are permanent magnets of different thicknesses, respectively; $Fm1$ and $Fm2$ are magnetomotive forces of permanent magnets of different thicknesses, respectively; R_σ is the permanent magnet magnetic leakage; R_δ is the air gap reluctance; Rt is the stator tooth reluctance; F_n is the armature magnetomotive force; Ry is the stator yoke reluctance. Φ_δ is for main flux and Φ_δ for leakage flux.

From the equivalent magnetic circuit structure diagram, it is clear that permanent magnets with

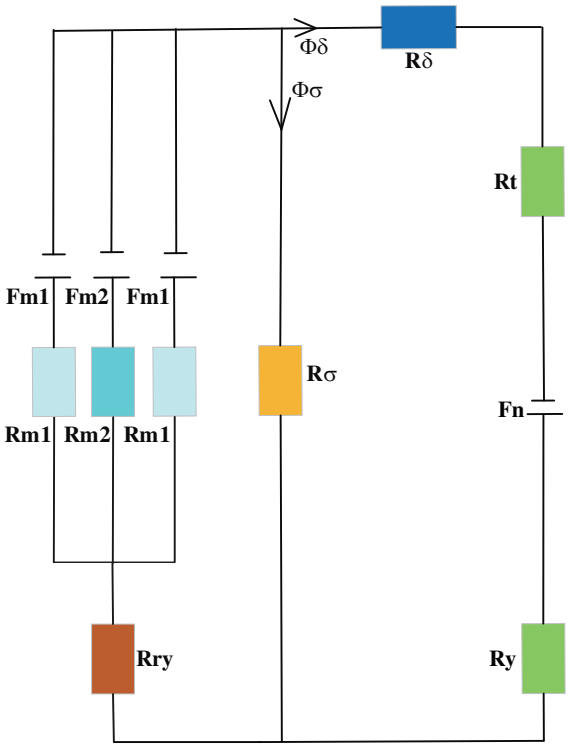

Figure 12. Magnetic circuit structure diagram.

different thicknesses have different magnitudes of magnetoresistance and magnetomotive force. The yoke and reluctance are in parallel to form a magnetic circuit, which generates a reverse electromotive force through a common turn-chain flux through the air gap in stator windings [31]. By changing the thickness of the permanent magnet, the flux density distribution of the air gap can be changed, which facilitates the sinusoidalization of the air gap magnetic field, and high sinusoidal inverse electromagnetic field waveforms can be obtained [32]. The unequal thickness pole structure can weaken the cogging torque of the motor.

4.3. Analysis of Electromagnetic Characteristics of Motor

To observe the changes in motor performance other than the cogging torque, this section compares the electromagnetic characteristics of two different permanent magnet structures before and after optimization, mainly analyzing the air-gap magnetic field, air-gap flux density, counter-electromotive force and its harmonics, and rotor mechanical strength.

4.3.1. Magnetic Field Distribution and Air Gap Flux Density

The no-load magnetic field distribution of AFIR motor with traditional structure and unequal thickness pole structure is shown in Fig. 13(a), and the 3D distribution of air gap flux density is shown in Fig. 13(b).

Compared with the initial structure, the rotor core with unequal-thickness pole structure has increased magnetic density, which increases the air-gap flux of the motor magnetic circuit. From Figs. 13(b) and (c), the air gap flux density of the unequal thickness pole structure is larger than

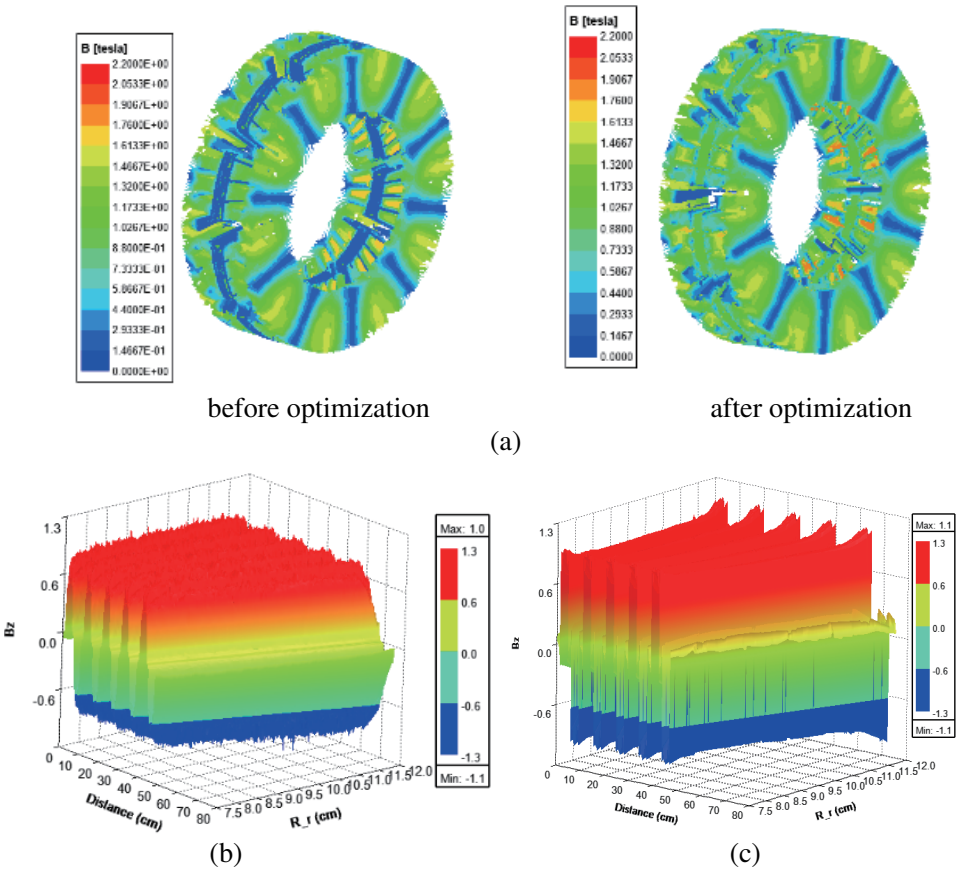

Figure 13. Air gap flux density. (a) Magnetic field distribution. (b) Initial structure. (c) Unequal thickness structure.

that of the initial structure. The maximum air gap flux density of the initial structure is 1.1 T, and the maximum air gap flux density of the unequal thickness pole structure is 1.3 T. The air gap magnetic field with unequal thickness of magnetic pole structure is more obvious in the direction of rotor radius (R_r in the figure).

4.3.2. Air Gap Midline Magnetic Flux Density

The air gap centerline was set up in the radial direction of the motor with the purpose of further observing the radial distribution of air gap flux density before and after optimization, which is shown in Fig. 14(a). R_i represents the inner diameter of the permanent magnet; R_o represents the outer diameter of the permanent magnet; R_r represents the radius at the midline of the air gap. Fig. 14(b) shows the air-gap flux density, and Fig. 14(c) shows the harmonic analysis of the air-gap flux density.

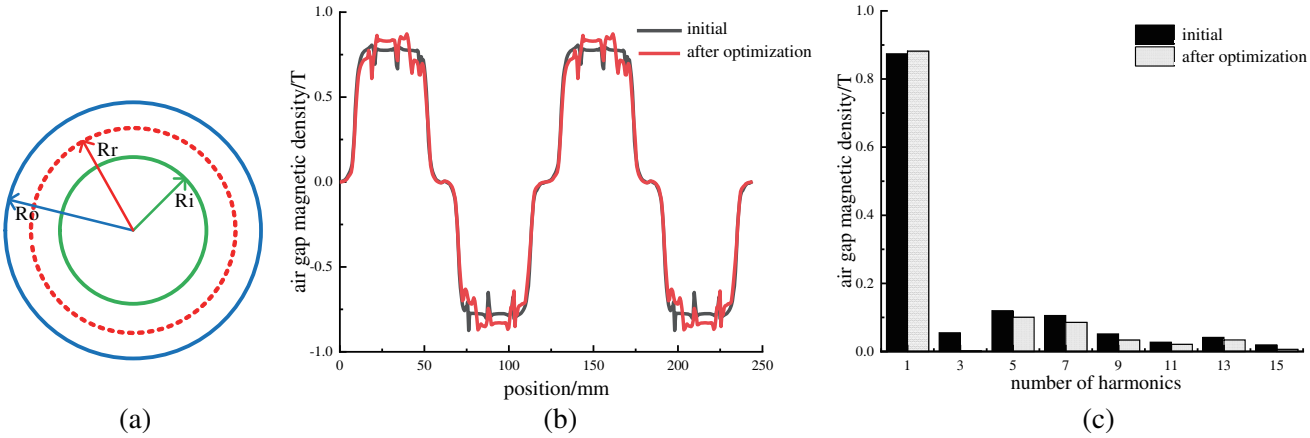

Figure 14. Air gap midline and air gap magnetic density.

From Fig. 14, the distribution trends of the air gap flux density of the two structures are approximately the same, and the air gap flux density of the unequal-thickness pole structure is larger, which is 0.8 T. The harmonic Fourier analysis plot 14(c) shows that the fundamental amplitude of the unequally thick pole structure is larger than that of the initial structure, and the 3rd, 5th, 7th, and 9th harmonics are reduced. The 3rd harmonic decreases the most, from 0.055 T to 0.0022 T, a decrease of 96%, and the other subharmonics also decrease slightly. According to the equations in [33], the air-gap conductive harmonic numbers of the 45-slot 10-pole motor are mainly the 1st and 3rd harmonics. Thus the 3rd harmonic drops the most, which is consistent with the simulation results.

4.3.3. Back EMF

The back EMFs of the initial rotor structure and the unequal thickness pole structure at 6000 rpm (taking phase A as an example) are compared and analyzed. The back EMF and back EMF harmonic analysis are shown in Fig. 15.

From Fig. 15, it can be seen that the reaction potential waveform of unequal thickness pole structure has better sinusoidality than the unoptimized one, with smoother curve and less data fluctuation.

The back EMF fundamental amplitude of the optimized pole structure was improved. The back EMF fundamental amplitude before optimization is 441 V and after optimization is 465 V. The back EMF fundamental amplitude of the unequal thickness pole structure is 5.4% higher, and the 3rd, 5th, 7th, and 9th harmonics are weakened to varying degrees. Among them, the 3rd harmonic is reduced by 16.4%, the 5th harmonic reduced by 32.1%, the 7th harmonic reduced by 77.1%, and the 9th harmonic reduced by 64%.

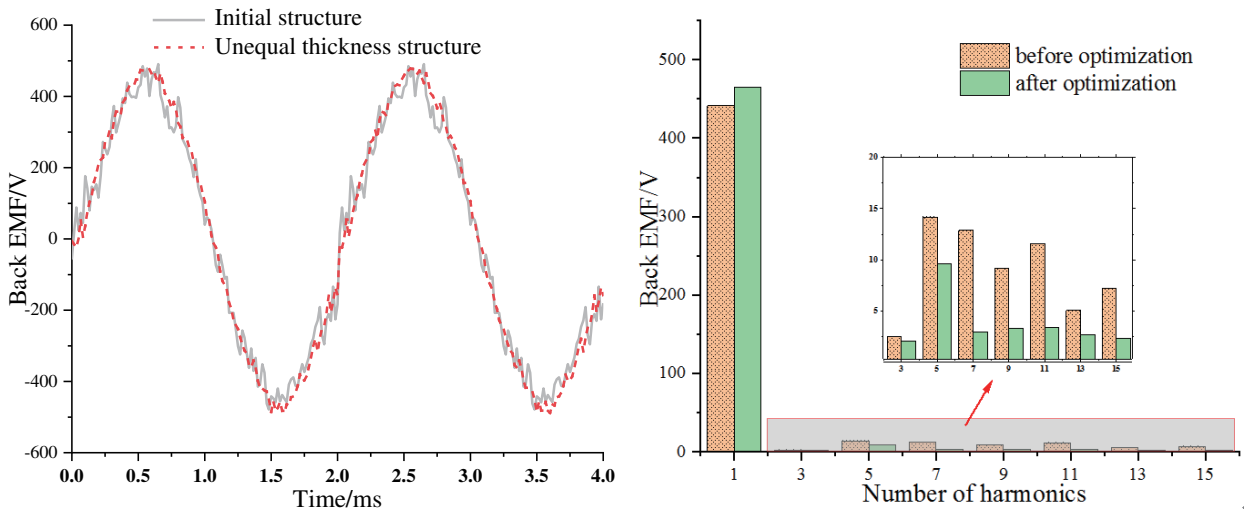

Figure 15. Back EMF and its harmonic analysis.

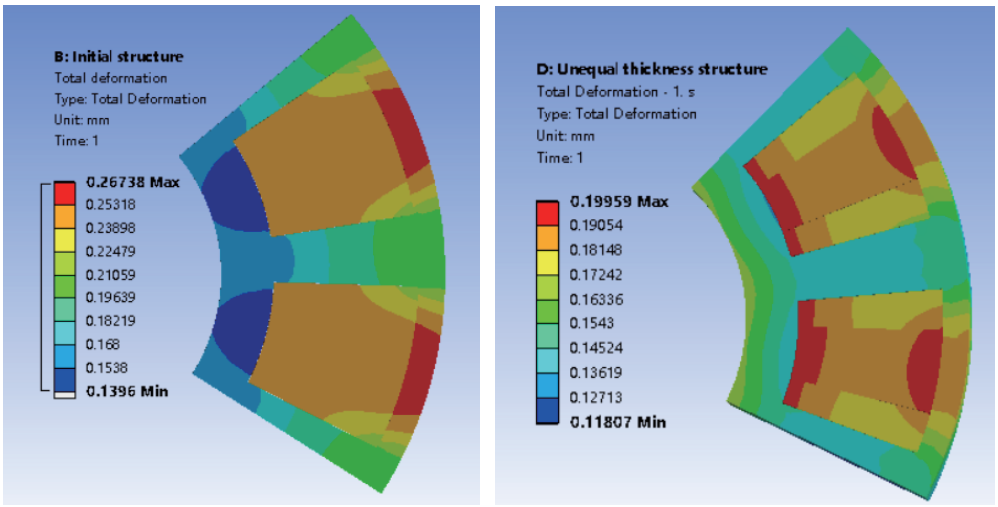

Figure 16. Total deformation.

4.3.4. Rotor Mechanical Strength Analysis

To observe the mechanical strength of the rotor before and after optimization, the total deformations and equivalent forces at 15,000 rpm of the rotor with the initial structure and unequal-thickness pole structure were compared. The total deformations and equivalent forces of the two structures are shown in Fig. 16 and Fig. 17, and the radial equivalence forces of the permanent magnets is shown in Fig. 18.

The total deformation of the rotor is shown in Fig. 16. The total deformation of the rotor of the initial structure and the unequal thickness pole structure is 0.28 mm and 0.31 mm, respectively. The deformation of the unequal-thickness pole structure is larger than the internal deformation at the diameter of the permanent magnet, which is caused by the unequal thickness of the edges of the permanent magnet. It can be seen that before and after optimization, the total deformation of the rotor is not large, and no sweeping phenomenon occurs.

The rotor core equivalent force is shown in Fig. 17. It can be seen that the maximum equivalent stress occurs on the rotor core, and the equivalent stress on the permanent magnet is much smaller. Because the permanent magnets are attached inside the rotor core and are supported by the rotor core,

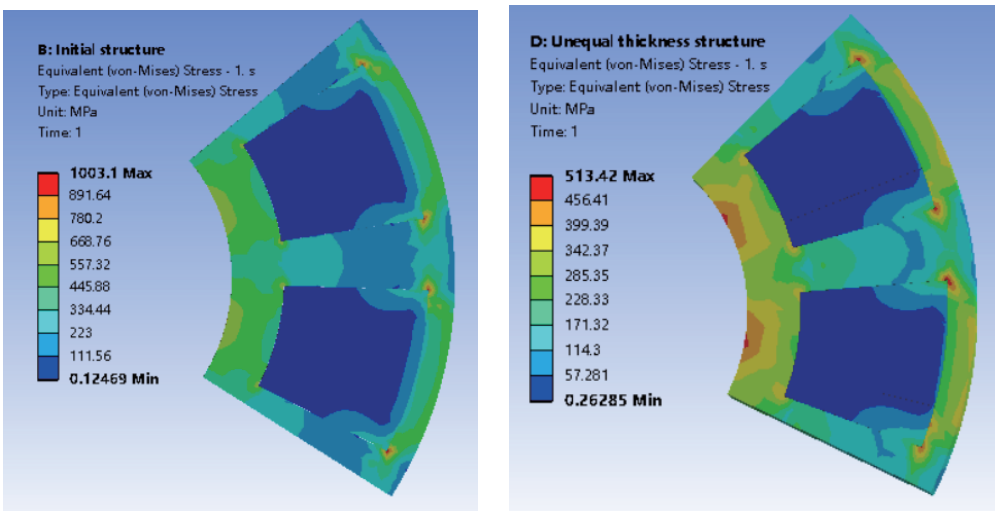

Figure 17. Rotor core equivalent force.

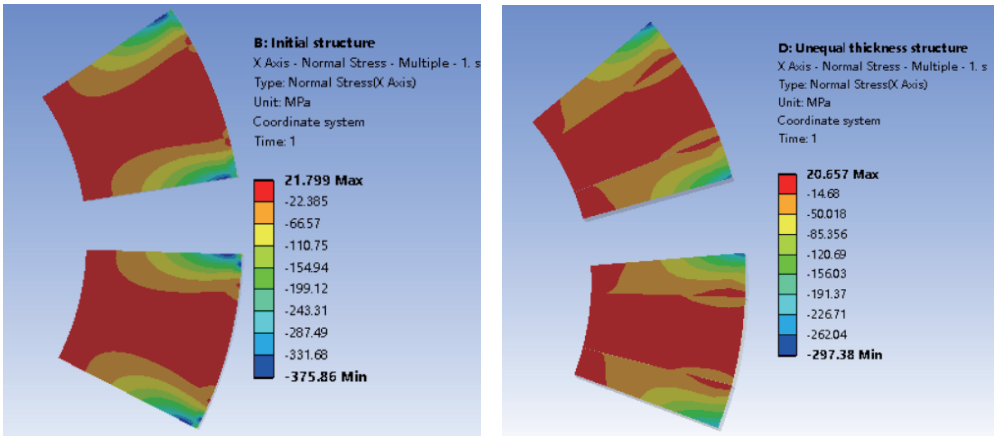

Figure 18. Radial equivalent force.

the rotor core carries the main force. After the optimized structure, the rotor core and permanent magnets and other effect forces are reduced.

The radial equivalent force of the permanent magnet is shown in Fig. 18. The permanent magnet material is Ndfe35, and its tangential and radial tension should be less than 80 Mpa [34]. The maximum radial stress of the initial structure and the unequal thickness structure is 21.8 Mpa and 20.7 Mpa, respectively, which is far less than 80 Mpa. Thus, the equivalent force generated by the high-speed rotation of the motor does not damage the structure of the permanent magnet.

5. COGGING TORQUE OPTIMIZATION RESULTS

Based on the previous section, 3D finite element models of the initial rotor structure and unequal thickness pole structure have been developed. Other electromagnetic characteristics have been compared in Section 4.3, and the analysis results of the cogging torque are as follows.

Firstly, the preliminary parameter scanning of h_a and h_b was carried out. It was found that h_a was between 7 mm and 7.5 mm, and h_b between 8.5 mm and 9 mm, and the cogging torque weakening effect was better. Then gradually narrow down the range until you find the optimal thickness combination.

Finally, h_a is determined between 7.42 mm and 7.45 mm, at which time the accuracy of the permanent magnet thickness has reached 0.01 mm, and there is no need to continue to narrow the range.

Through simulation experiments, the experimental results shown in Table 2 are obtained. Based on the data in Table 2, the torque amplitude and torque ripple (Kt) curves of the tooth grooves at different thicknesses were plotted as shown in Fig. 19. Fig. 20 shows the cogging torque diagram of the AFIR motor with an unequal-thickness pole structure for the initial structure and the optimal combination of thicknesses.

Table 2. Simulation results.

h_a/mm	h_b/mm	amplitude/Nm	T_{avg}/Nm	k_t
8	8	2.06	145.13	9.51%
7	9	1.51	149.29	6.78%
7.1	8.9	1.18	146.11	6.57%
7.2	8.8	.87	145.77	7.18%
7.3	8.7	.59	145.71	7.05%
7.4	8.6	0.35	147.58	7.95%
7.5	8.5	0.46	146.14	6.26%
7.42	8.58	0.32	145.88	7.80%
7.43	8.57	0.39	149.18	6.84%
7.44	8.56	0.38	146.69	7.73%
7.45	8.55	0.28	147.26	6.78%

Table 3. Motor test data (partial).

Rotation speed	Current (A)	Input Power (W)	Output power (W)	Efficiency (%)
100	29.25	2468	2093.6	84.8
100	54.62	4735	4187.2	88.4
100	80.54	7095	6270.3	88.4
100	107.77	9600	8384.8	87.3
100	136.27	12270	10510	85.7
100	165.42	15060	12582	83.5
100	196.81	18140	14707	81.1
100	233.39	21520	16823	78.2
100	266.87	25010	18791	75.1
100	305.22	29150	20810	71.4
100	339.61	33410	22485	67.3
2000	220	361.84	58980	46103
3000	215	342.12	79810	67527
4200	164	269.69	80020	71892
5000	140	260.87	80850	73181
6000	80	144.05	53370	50063

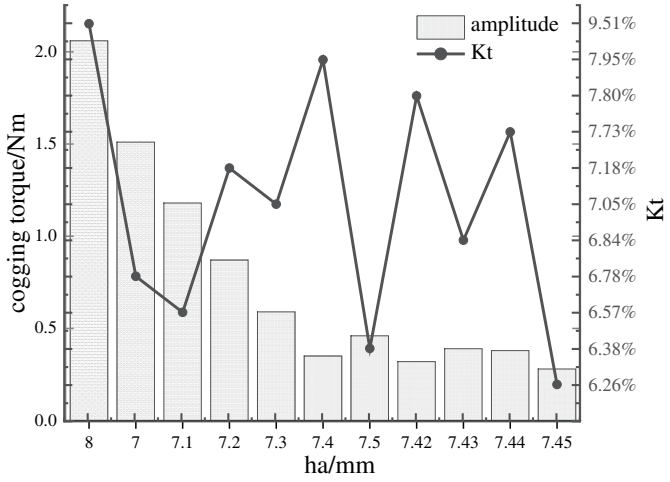

Figure 19. Torque amplitude and torque ripple.

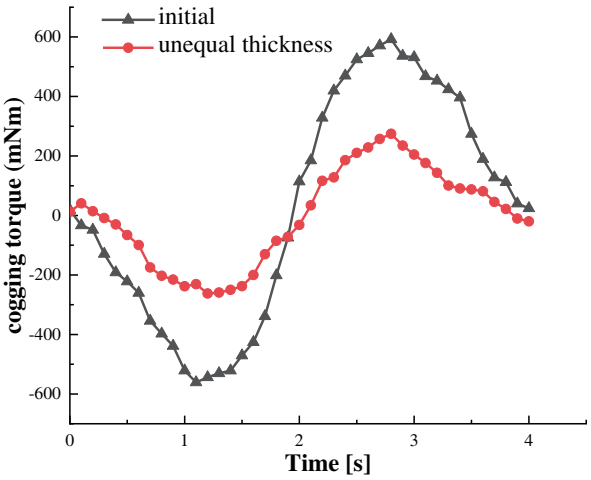

Figure 20. Cogging torque.

Figure 20 shows the cogging torque diagram of the AFIR motor with unequal-thickness pole structure for the initial structure and the optimal thickness combination. When the thicknesses of the middle and both sides of the unequal-thickness pole are 7.45 mm and 8.55 mm, respectively, the tooth slot torque is the smallest. The peak cogging torque of the motor with the two pole structures is 2.06 Nm and 0.28 Nm, respectively. The cogging torque is greatly reduced by 86.4%, and the torque ripple is reduced by 8.73%, indicating a good optimization effect.

6. PROTOTYPE TEST

To verify the correctness of the theoretical analysis and three-dimensional finite element analysis, the motor was tested, and the experimental platform is shown in Fig. 21. Fig. 22 shows the variation rule of motor efficiency with input current under the same rotational speed. Fig. 23 shows the distribution of motor efficiency. Table 3 shows the data obtained from the test.

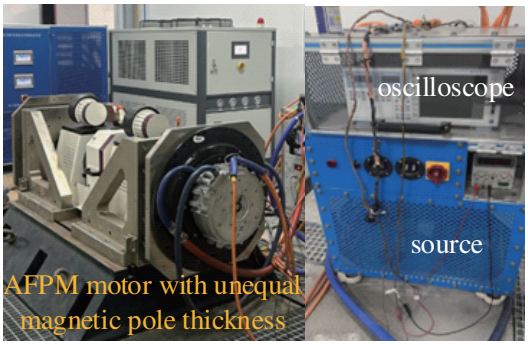

Figure 21. Experimental platform.

Data in Fig. 22 are obtained from Table 3. In Fig. 22, the motor is divided into six groups, with speeds ranging from 1000 rpm to 6000 rpm, and the changes in motor efficiency with input current are observed within each group. From the experimental results, as the current increases, the motor efficiency increases and then decreases; when the motor speed is between 4000 rpm and 6000 rpm, the motor efficiency is the highest, which can be more than 94%. From Fig. 23, the motor efficiency is highest when the motor torque is between 4000 and 6000 rpm.

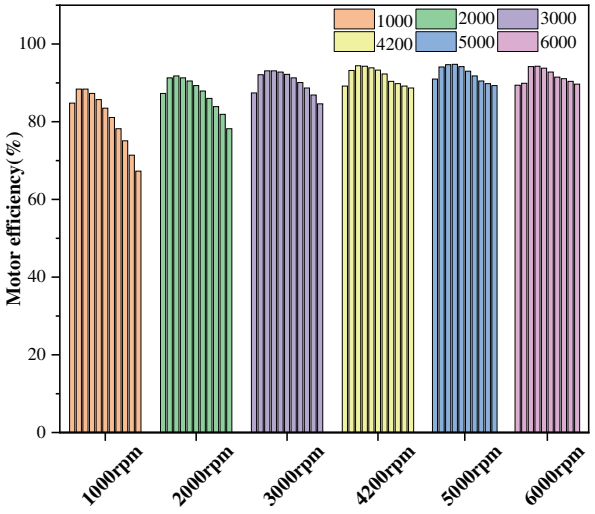

Figure 22. Efficiency at different speeds.

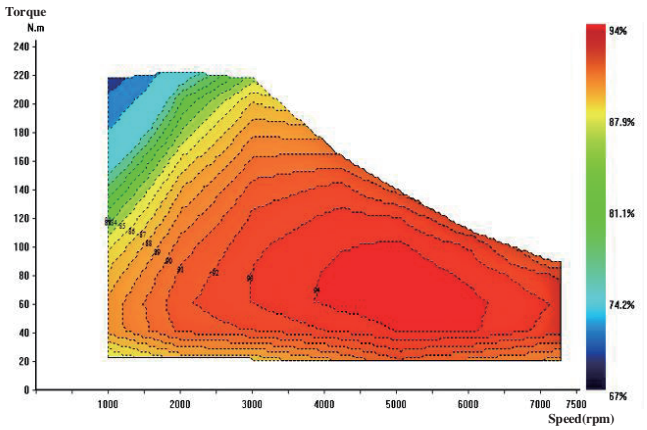

Figure 23. Efficiency distribution chart.

7. CONCLUSION

In this paper, a three-phase 45 KW, 10-pole, 45-slot AFIR motor is taken as an example to compare the effects of different pole optimization methods on the cogging torque, derive the mathematical formula for the cogging torque of the AFIR motor, and explain the principle of the unequal-thickness poles weakening the cogging torque. The changes in the motor characteristics, including the magnetic field distribution, air-gap flux density, reverse electromotive force, and rotor stresses, after the magnetic poles adopt the unequal-thickness structure are compared. The main conclusions obtained are as follows:

(1) Various pole optimization methods (axial segmentation, radial segmentation, and unequal thickness structure) influence the motor slot torque, and among the three of them, unequal thickness pole structure has the best effect.

(2) The unequal thickness structure of magnetic poles will change the center of the inner and outer diameters of the magnet, thus generating eccentricity. By reasonably designing the thickness of permanent magnets and changing the eccentricity distance, the cogging torque expression coefficient can be reduced, and the cogging torque can be weakened.

(3) The optimized air-gap flux density curve and motor no-load reverse electromotive force waveform have better sinusoidality, and the various harmonics are reduced, which has a better optimization effect.

(4) Compared with the initial structure, the total deformation of the optimized rotor is not much different; the rotor equivalent force is slightly reduced; and the radial stress of the optimized permanent magnets is reduced and much lower than the permissible value, which ensures the mechanical strength of the rotor and permanent magnets.

(5) With the unequal thickness structure, the cogging torque is reduced by about 86.4%; the output torque is increased by 1.5%; and the torque ripple is reduced by 8.73%, which has a better optimization effect.

Therefore, the optimization method of unequal thickness pole structure can significantly reduce the cogging torque of the AFIR motor with less effect on the output torque, and also slightly reduce the torque ripple, which is effective.

REFERENCES

1. Liu, X. P., D. Chen, M. Wang, Y. F. Huang, and Q. H. Xie, "Analysis of mechanical dynamics and flux weakening ability for a variable flux axial field permanent magnet electrical machine," *Trans. Chin. Eletrotechnol. Soc.*, Vol. 31, 54–62, 2016.

2. Luo, X. and S. Niu, "Maximum power point tracking sensorless control of an axial-flux permanent magnet verneer wind power generator," *Energies*, Vol. 9, 581, 2016.
3. Shi, Z., X. Sun, Y. Liu, and W. Zhou, "Fault-tolerant model predictive current control of five-phase permanent magnet synchronous hub motor considering current constraints," *Proceedings of the 2020 IEEE Vehicle Power and Propulsion Conference (VPPC)*, 1–5, Gijon, Spain, Nov. 18–Dec. 16, 2020.
4. Ji, J. H., Y. K. Sun, J. H. Zhu, and W. X. Zhao, "Design, analysis and experimental validation of a modular permanent-magnet machine," *Trans. Chin. Eletrotechnol. Soc.*, Vol. 30, 243–252, 2015.
5. Deng, W. and S. Zuo, "Analytical modeling of the electromagnetic vibration and noise for an external-rotor axial-flux in-wheel motor," *IEEE Trans. Ind. Electron.*, Vol. 65, 1991–2000, 2018.
6. Kumar, P. and R. K. Srivastava, "Influence of rotor magnet shapes on performance of axial flux permanent magnet machines," *Progress In Electromagnetics Research*, Vol. 85, 155–165, 2018.
7. Neethu, S., S. P. Nikam, and S. Sikam, "High-speed coreless axial-flux permanent-magnet motor with printed circuit board winding," *IEEE Trans. Ind. Appl.*, Vol. 55, 1954–1962, 2019.
8. Wanjiku, J., M. A. Khan, P. S. Barendse, et al., "Influence of slot openings and tooth profile on cogging torque in axial-flux PM machine," *IEEE Transactions on Industrial Electronics*, Vol. 62, No. 12, 7578–7589, 2015
9. Gieras, J. F., R. J. Wang, and M. Kamper, *Axial Flux Permanent Magnet Brushless Machines*, Springer-Verlag, 153–155, New York, 2008.
10. Sun, M. C., R. Y. Tang, X. Y. Han, et al., "Analysis and modeling for open circuit air gap magnetic field prediction in axial flux permanent magnet machines," *Proceedings of the CSEE*, Vol. 38, No. 5, 1525–1533, 2018.
11. Gieras, J. F., R. J. Wang, and M. Kamper, *Axial Flux Permanent Magnet Brushless Machines*," Springer Verlag, 29–34, New York, 2008.
12. Tang, R. Y, *Modern Permanent Magnet Motor: Theory and Design*, 308–314, Machinery Industry Press, 1997.
13. Zhang, L., X. Y. Zhu, and Y. F. Zuo, "Overview of fault-tolerant technologies of rotor permanent magnet brushless machine and its control system for electric vehicles," *Proceedings of the CSEE*, Vol. 39, No. 6, 1792–1802, 2019
14. Yazdani-Asrami, M., W. Song, M. Zhang, W. Yuan, and X. Pei, "Magnetization loss in HTS coated conductor exposed to harmonic external magnetic fields for superconducting rotating machine applications," *IEEE Access*, Vol. 9, 77930–77937, 2021.
15. Shi, Z., X. Sun, Y. Cai, Z. Yang, G. Lei, Y. Guo, and J. Zhu, "Torque analysis and dynamic performance improvement of a PMSM for EVs by skew angle optimization," *IEEE Trans. Appl. Supercond.*, Vol. 29, 1–5, 2019.
16. Lei, G., G. Bramerdorfer, B. Ma, Y. Guo, and J. Zhu, "Robust design optimization of electrical machines: Multi-objective approach," *IEEE Trans. Energy Convers.*, Vol. 36, 390–401, 2021.
17. Wang, M., C. Tong, Z. Song, et al., "Performance analysis of an axial magnetic field modulated brushless double rotor machine for hybrid electric vehicles," *IEEE Transactions on Industrial Electronics*, Vol. 66, No. 4, 806–817, 2019.
18. Guo, B., Y. Huang, F. Peng, et al., "Analytical modeling of misalignment in axial flux permanent magnet machine," *IEEE Transactions on Industrial Electronics*, Vol. 67, No. 6, 4433–4443, 2020.
19. Yang, Y. B., X. H. Wang, X. Zhang, et al., "Cogging torque reduction method of magnet shifting in permanent magnet motors," *Transactions of China Electrotechnical Society*, Vol. 21, No. 10, 22–25, 2006.
20. Huang, Y. K., T. Zhou, J. N. Dong, et al., "A review of axial permanent magnet motors and their research and development," *Proceedings of the CSEE*, Vol. 35, No. 1, 192–205, 2015.
21. Wu, S. S., B. J. Wang, T. Zhang, and Q. H. Gu, "Design optimization and electromagnetic performance analysis of an axial-flux permanent magnet brushless dc motor with unequal-thickness magnets," *Appl. Sci.*, Vol. 12, No. 15, 7863, 2022.

22. Ni, Y. Y., L. Wang, and Q. J. Wang, "Modeling and analysis of convex unequal-thickness pole permanent magnet motor," *Journal of Electrotechnology Journal of Electrotechnology*, Vol. 35, No. 11, 2406–2414, 2020.
23. Ni, Y. Y., L. Wang, and M. M. Ge, "Analytical modeling and optimization of three-section unequal thickness Halbach permanent magnet motor," *Journal of Hefei University of Technology (Natural Science Edition*, Vol. 43, No. 3, 349–357, 2020.
24. Li, J. Z., X. Z. Wu, and C. T. Chen, "Analytical calculation of air-gap magnetic field of permanent magnet motor based on magnetic pole segmentation," *Chinese Journal of Electrical Engineering*, Vol. 41, No. 18, 6390–6399, 2021.
25. Liu, F., T. Deng, and X. B. Hua, "Research on electromagnetic structure design and heat dissipation of disc permanent magnet synchronous motor," *Journal of Chongqing University of Technology (Natural Sciences)*, Vol. 35, No. 12, 77–84, 2021.
26. Hao, L., M. Y. Lin, D. Xu, et al., "Cogging torque reduction in axial field flux-switching permanent magnet machines," *Transactions of China Electrotechnical Society*, Vol. 30, No. 2, 21–26, 2015.
27. Tao, C. X., M. L. Fu, F. Y. Gao, et al., "Effects of auxiliary slots on the torque of an interior permanent-magnet synchronous motor," *Journal of Chongqing University*, Vol. 44, No. 4, 64–76, 2021.
28. Zhang, X. C., X. Y. Yang, and J. H. Cao, "Performance analysis of permanent magnet brushless DC motor with unequal thick magnetic poles," *Micro Motor*, Vol. 42, No. 2, 9–13, 2014,
29. Xu, Y. L., L. J. Xu, and Q. L. Gao, "Size equation and magnetic network model of yoke block armature axial magnetic field permanent magnet motor," *Electric Machines and Control*, Vol. 23, No. 11, 27–32, 2019
30. Gong, X. and Y. L. Xu, "Lumped parameter magnetic circuit analysis of axial flux permanent magnet motor and its analytical calculation of air gap leakage," *Electric Machines and Control*, Vol. 17, No. 10, 59–64, 2013.
31. Xu, L., X. Y. Zhu, C. Zhang, et al., "Torque quality analysis and optimization design of magnetic pole radial combined axial magnetic field permanent magnet motor," *Proceedings of the CSEE*, Vol. 41, No. 6, 1971–1983, 2021.
32. Xie, Y. and C. M. Qu, "Design and study of disc coreless motor with trapezoidal permanent magnet," *Electric Machine and Control*, Vol. 20, No. 8, 7482, 2016.
33. Liu, J. Q., J. G. Bai, P. Zheng, G. P. Liu, and J. X. Huang, "Research on cogging torque based on magnetic field modulation principle," *Journal of Electrotechnology*, Vol. 35, No. 5, 931–941, 2020.
34. Gao, F. Y., X. D. Qi, X. F. Li, et al., "Analytical calculation and optimization analysis of electromagnetic performance of Halbach partial segmented permanent magnet synchronous motor of unequal width and thickness," *Transactions of China Electrotechnical Society*, Vol. 37, No. 6, 1398–1414, 2022.